PCCP

Interleaflet Coupling of n-Alkane Incorporated Bilayers

Journal:	*Physical Chemistry Chemical Physics*
Manuscript ID	CP-ART-11-2019-006059.R1
Article Type:	Paper
Date Submitted by the Author:	18-Dec-2019
Complete List of Authors:	Usuda, Hatsuho; University of Tsukuba, Chemistry Hishida, Mafumi; University of Tsukuba, Department of Chemistry Kelley, Elizabeth; National Institute of Standards and Technology, Center for Neutron Research Yamamura, Yasuhisa; University of Tsukuba, Chemistry Nagao, Michihiro; NIST, NCNR; Indiana University, CEEM Saito, Kazuya; University of Tsukuba, Chemistry

PCCP

ARTICLE TYPE

Cite this: DOI: 00.0000/xxxxxxxxxx

Interleaflet Coupling of *n*-Alkane Incorporated Bilayers

Hatsuho Usuda,[a] Mafumi Hishida,[a] Elizabeth G. Kelley,[b] Yasuhisa Yamamura,[a] Michihiro Nagao,*[b,c] and Kazuya Saito*[a]

Received Date
Accepted Date

DOI: 00.0000/xxxxxxxxxx

The relationship between the membrane bending modulus (κ) and compressibility modulus (K_A) depends on the extent of coupling between the two monolayers (leaflets). Using neutron spin echo (NSE) spectroscopy, we investigate the effects of *n*-alkanes on the interleaflet coupling of 1,2-dipalmitoyl-*sn*-glycero-3-phosphocholine (DPPC) bilayers. Structural studies with small-angle X-ray and neutron scattering (SAXS and SANS) showed that the bilayer thickness increased with increasing *n*-alkane length, while NSE suggested that the bilayers became softer. Additional measurements of the membrane thickness fluctuations with NSE suggested that the changes in elastic moduli were due to a decrease in coupling between the leaflets upon addition of the longer *n*-alkanes. The decreased coupling with elongating *n*-alkane length was explained based on the *n*-alkane distribution within the bilayers characterized by SANS measurement of bilayers composed of protiated DPPC and deuterated *n*-alkanes. A higher fraction of the incorporated long *n*-alkanes were concentrated at the central plane of the bilayers and decreased the physical interaction between the leaflets. Using NSE and SANS, we successfully correlated changes in the mesoscopic collective dynamics and microscopic membrane structure upon incorporation of *n*-alkanes.

1 Introduction

Lipids are a primary ingredient of biological membranes and the function of several membrane proteins are influenced by the physical properties of the underlying lipid bilayer. For example, the lipid membrane mechanical properties, such as the membrane tension and bending modulus (κ), are known to significantly affect the activity of ion channels.[1] Also, the diffusion of peripheral proteins is affected by the membrane viscosity and the intermonolayer coupling which is related to the friction between two monolayers (leaflets) that opposes sliding of the individual monolayers relative to one another. These essential membrane properties are determined by the composition of lipids as well as the presence of other small molecules; however, the effects of additives on the membrane structure and dynamics are not well understood and not easily predicted.

Many organic molecules other than lipids participate in regulating the mechanical and physicochemical properties of biological membranes such as structure, elasticity and phase behavior.[2–12] Yet, a systematic understanding of the effects of small organic molecules on the membrane properties has not been fully realized. Significant research efforts have been devoted to understanding the effects of cholesterol, which is known to loosen molecular packing in the gel phase and lower the phase transition temperatures of lipid bilayers.[2–5,8] Less is known about other classes of organic molecules.

Our group has focused on the effects of *n*-alkanes, where both the *n*-alkane length and concentration within the membrane systematically change the membrane properties.[9–12] The effects of *n*-alkanes on lipid membranes have been studied for more than 30 years because of their known anaesthetic properties as well as their use in black lipid membranes.[13–17] *n*-Alkanes with 12 and 14 carbons have the opposite effect to cholesterol on the molecular packing and the phase transition temperatures of lipid bilayers, specifically they tighten the molecular packing in the gel phase and increase the phase transition temperature.[10,13] In contrast, the main transition temperature decreases when *n*-alkanes shorter than C12 are incorporated into lipid membranes.[10,13] The location of *n*-alkanes within the bilayer can also depend on the carbon length.[13,18] Absorption of *n*-alkanes into the center of a bilayer leads to substantial changes in the bilayer thickness but only minor changes in the area per lipid,[19,20] while absorption of *n*-alkanes parallel to the lipid tails leads to a smaller increase in bilayer thickness. As there is a well-known chain length dependence to the effects on the lipid main transition temperature and the alkane distribution within the bilayer, we expect that chain length of *n*-alkane within the membrane would also affect the membrane dynamics and associated mechanical properties,

[a] *Department of Chemistry, Faculty of Pure and Applied Sciences, University of Tsukubas, Tsukuba, Ibaraki 305-8571, Japan. E-mail : kazuya@chem.tsukuba.ac.jp*
[b] *National Institute of Standards and Technology (NIST) Center for Neutron Research, National Institute of Standards and Technology,Gaithersburg, MD, 20899-6102 USA.*
[c] *Center for Exploration of Energy and Matter, Indiana University, Bloomington, IN, 47408-1398, USA. E-mail : mnagao@indiana.edu*

as well as the interleaflet coupling, which is focus of the current paper.

The relation between the membrane bending (κ) and compressibility moduli (K_A) is well established theoretically and described by a coupling constant β.[21,22] The value of β increases as the leaflets decouple and the bilayer behaves more like two independent monolayers. The effects of additives on this coupling is not well known, in part because determining β requires an independent measure of both κ and K_A. Work by Shchelokovskyy *et al*. used a combination of micropipette aspiration and fluctuation analysis to determine the effects of HIV-1 fusion peptide on the elastic properties of model lipid bilayers.[23] They found that the HIV-1 fusion peptide increased β, implying that the leaflets were less coupled compared to the pure lipid bilayer. The authors suggested that the presence of the peptide in the hydrophobic center of the bilayer pushed the leaflets apart and significantly reduced the interactions between the two lipid leaflets.

In this study, we vary the *n*-alkane length to systematically investigate the effects of small molecule additives on the elastic moduli and the coupling in model lipid bilayers. We use small-angle X-ray scattering (SAXS) and small-angle neutron scattering (SANS) techniques to characterize the bilayer structure with added *n*-alkane and explore the location of the *n*-alkane within the hydrophobic bilayer core. We characterize the membrane dynamics using neutron spin echo (NSE) spectroscopy to measure both the collective bending and thickness fluctuations and determine κ and K_A.[24] The combined results show that β increases when the *n*-alkanes are located within the central plane of the bilayer. These results support the idea that decreasing the interactions between leaflets decreases the coupling between leaflets, with the added *n*-alkane acting as a lubricant and softening the membrane.

2 Theory

NSE experiments directly measure the intermediate scattering function, $I(q,t)$ as a cosine Fourier transform of the scattering law, $S(q,\omega)$, where $q = 4\pi\sin\theta/\lambda$ is the magnitude of the scattering vector, 2θ and λ are the scattering angle and the wavelength of the incident neutron, ω is the exchanged energy and t is the Fourier time, that is a time associated with the exchanged energy ω. Zilman and Granek (ZG)[25] derived the expression for $I(q,t)$ to describe membrane fluctuations based on the Helfrich model for bending energy,[26]

$$\frac{I(q,t)}{I(q,0)} = \exp\left[-(\Gamma t)^{\frac{2}{3}}\right] \tag{1}$$

where Γ is the relaxation rate and follows a q^3 dependence, $\Gamma \propto q^3$. When protiated bilayers are subjected to measurements in D_2O by NSE, it is well documented that $I(q,t)$ follows the predicted scaling.[27–29] Watson and Brown[30] included the effects of the internal dissipation within the bilayer into the ZG formalism to better describe the dynamics observed on the nanoscale with NSE.[31] Nagao and colleagues proposed a relationship between Γ measured with NSE and the membrane bending modulus κ by incorporating these theoretical considerations as,[24,32]

$$\Gamma = 0.0069\sqrt{\frac{k_BT}{\kappa}}\frac{k_BT}{\eta}q^3 \tag{2}$$

where k_BT is the thermal energy and η is the viscosity of the solvent (D_2O). This expression allows us to determine the κ from the dynamics observed for the lipid bilayers with added *n*-alkanes.

When a bilayer bends, one monolayer experiences expansion while the other is compressed. This mechanical relation is expressed in a thin elastic sheet model as,

$$\kappa = \frac{K_A}{\beta}{d_c}^2 \tag{3}$$

where K_A is the bilayer area compressibility modulus, β is a coupling constant between two monolayers, and d_c is the hydrocarbon thickness of the bilayer. Experimentally, d_c can be obtained either from SAXS or SANS measurements, while K_A and β are not readily measurable for large unilamellar vesicles (LUVs). It is noted that lipid chemistry affects both the head group and tail regions of the bilayer and they contribute differently to κ. The impact of the tail region is seen directly in changes in ${d_c}^2$. On the other hand, head group modification as well as tail packing and interactions can affect the value of κ through changes in K_A and/or β.

Recently, K_A was estimated from NSE measurements of LUVs by taking advantage of contrast matching. These measurements require contrast matching the hydrophobic tails to the surrounding solvent and emphasizing the coherent dynamics of the lipid headgroups.[24,33–35] At this contrast, $I(q,t)$ followed Eq. 1, while Γ shows a distinct deviation from the underlying q^3 dependence.[36–38] The "excess" dynamics were interpreted as the thickness fluctuations of the bilayers, and Γ was expressed by the superposition of the bending and thickness fluctuations[24] as,

$$\frac{\Gamma}{q^3} = 0.0069\sqrt{\frac{k_BT}{\kappa}}\frac{k_BT}{\eta} + \frac{(\tau_{TF}{q_0}^3)^{-1}}{1+(q-q_0)^2\xi^2}. \tag{4}$$

The first term is the same as Eq. 2, and originates from the membrane bending fluctuations, and the second term is a phenomenological expression for the thickness fluctuations, where q_0 is the peak position of the Lorentz function, τ_{TF} is the relaxation time of the thickness fluctuations, and ξ^{-1} is the half-width at the half maximum of the peak, respectively. The peak maximum of the excess dynamics, q_0, corresponds to the first minima in the bilayer form factor measured with SANS and is associated with the bilayer thickness.

Here, our focus is on the parameter ξ^{-1} which is related to the amplitude δd_c of the thickness fluctuations.[24,35,36,38–41] The fractional change in the thickness can be defined as,

$$\sigma_d = \frac{\delta d_c}{d_c} = (q_0\xi)^{-1}. \tag{5}$$

By statistical mechanics, K_A is related to the fractional change in area $\sigma_A = \Delta A/A$ as,[42]

$$K_A = \frac{k_BT}{{\sigma_A}^2 A_0}, \tag{6}$$

where A and A_0 are the unit area of the membrane and the area per molecule, respectively. Assuming the volume compressibility is negligible ($V = Ad_c, \Delta V/V \approx \Delta A/A + \Delta d_c/d_c \approx 0$ where V is the volume), σ_A is equal to the fractional change in the thickness σ_d, i.e., ${\sigma_A}^2 = {\sigma_d}^2 = (\delta d_c/d_c)^2$.[42] Therefore, the experimental $q_0\xi$ relates to K_A as,

$$q_0\xi = \sqrt{\frac{K_A A_0}{k_B T}} \propto \sqrt{K_A}. \quad (7)$$

Thus, the thickness fluctuation amplitude is related to K_A, allowing us to explore the effects of added n-alkanes on both κ and K_A as well as the coupling between the two moduli.

3 Methods

Sample preparation

Protiated and tail-deuterated 1,2-dipalmitoyl-*sn*-glycero-3-phosphocholine (DPPC) were purchased from Avanti Polar Lipids (Alabaster, AL). Protiated and deuterated n-alkanes (octane (C8), decane (C10), dodecane (C12), tetradecane (C14)) were purchased from Sigma Aldrich (Darmstadt, Germany) and Cambridge Isotope Laboratories (Tewksbury, MA), respectively. D_2O was also purchased from Cambridge Isotope Laboratories. All the chemicals were used without further purification. Liquid n-alkane was added to DPPC powder at the molar ratio of DPPC : n-alkane $= 6:4$. The mixtures of DPPC and n-alkanes were dissolved in D_2O to give a lipid concentration of 100 mg/mL and sonicated for 3 h at 60 °C in an ultrasonic bath to ensure that the same n-alkanes ratio was incorporated in each system. Successful incorporation of n-alkanes was confirmed using differential scanning calorimetry (DSC) based on the absence of the thermal anomaly due to melting of pure n-alkane and change in the phase transition temperature of DPPC, which depends on the incorporation ratio.[9,12] After sonication, the samples were extruded through two stacked polycarbonate membranes with a nominal pore size of 100 nm using a heated Mini-Extruder and stored at 60 °C until the measurement.

Combinations of protiated and deuterated chemicals were chosen to get appropriate samples for each measurement. For SAXS experiments, fully protiated bilayers (protiated lipid and n-alkanes) were dispersed in H_2O. The contrast for X-ray scattering, which originates from the electron density (ED) profile, is shown in Fig. 1a. To more precisely locate the incorporated n-alkane in the bilayers, we used deuterated n-alkanes with protiated DPPC in D_2O. The scattering length density (SLD) profile for the neutron scattering at this contrast condition is shown in Fig. 1b. The bending fluctuations were observed using NSE by measuring fully protiated bilayers dispersed in D_2O with the corresponding SLD profile shown in Fig. 1c. The thickness fluctuations were captured by NSE using the headgroup-highlighted samples, where tail-deuterated DPPC and deuterated n-alkanes were used to contrast match the hydrophobic region of the bilayer to the D_2O solvent. As shown in Fig. 1d, only the head groups are protiated and visible in the scattering experiment. Small amounts of protiated DPPC and n-alkanes were added to tail deuterated DPPC and deuterated n-alkane to precisely match the SLD of the hydrophobic region with the carrier solvent, D_2O.

The samples with protiated DPPC (Fig. 1a,b,c) were subjected to measurements at 54 °C, while the samples with the tail-contrast-matched bilayers (Fig. 1d) were subjected to measurements at 50 °C. This differnece is because mechanical properties of lipid membranes change as a function of the reduced temperature $T - T_m$ where T_m is the main transition temperature of the lipid bilayers,[43] and T_m using tail-deuterated DPPC was found to be 4 °C lower than that using protiated DPPC.[44]

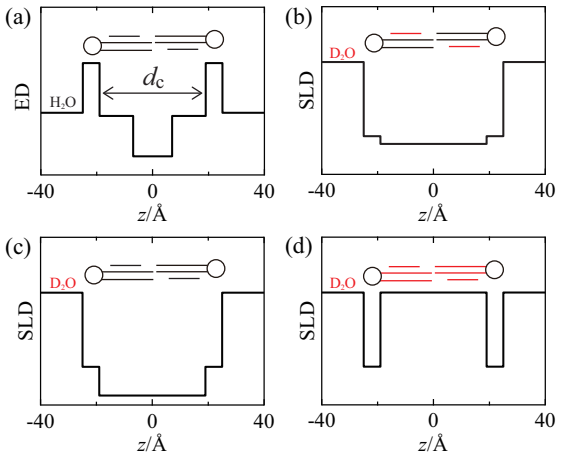

Fig. 1 Schematics of the scattering contrasts used to measure the structure and dynamics of the DPPC bilayers with added n-alkanes. Black portions of the molecule contain H atoms, while red parts are deuterated. (a) The electron density (ED) profile of fully protiated bilayers (protiated lipid and n-alkanes) in H_2O for SAXS measurements. (b) The scattering length density (SLD) profile of bilayers composed of protiated DPPC and deuterated n-alkanes in D_2O prepared for SANS. (c) The SLD profile of fully protiated bilayers in D_2O. (d) The SLD profile of the headgroup-highlighted bilayers (that is, the tail-contrasted-matched samples) mainly composed of tail-deuterated lipid and deuterated n-alkanes in D_2O, which were used for NSE and SANS.

Differential scanning calorimetry (DSC)

DSC measurements were performed using a commercial apparatus (Q200, TA Instruments, New Castle, DE). To see the thermal anomaly clearly, we used samples before extrusion which contain multilamellar vesicles. About 5 μL of the fully protiated samples were sealed in aluminum pans. Cooling and heating cycles were performed three times between 20 °C and 55 °C using a scan rate of 5 °C min^{-1} for the first ramp and 2 °C min^{-1} for the remaining ramps. The enthalpy change upon the transitions could not be determined because the amount of the bilayers in a pan was unknown due to poor uniformity of the suspension.

Small-angle X-ray scattering (SAXS)

SAXS experiments were conducted on BL10C in the Photon Factory, KEK, Japan, where PILATUS 2M (DECTRIS Ltd., Baden, Switzerland) detector and an incident X-ray with a wavelength of 1.5 Å were used. The measured q range was 0.013 Å^{-1} to 0.83 Å^{-1} at a sample-to-detector distance of 1.1 m. A silver behenate standard was used to calibrate sample-to-detector distances. A polyimide tube containing a sample was held in a hot stage

(FP900, Mettler-Toledo Inc., Columbus, OH) and all the samples were subjected to measurements at $T = 54$ °C. Data reduction was performed using Nika[45] and background correction was made by subtracting the SAXS profile of H_2O.

Small-angle neutron scattering (SANS)

SANS experiments were conducted on the NG7 30 m SANS at the National Institute of Standards and Technology (NIST), USA.[46,47] The incident neutron wavelengths λ were 8.9 Å and 6.0 Å, and the covered q range was from 0.001 Å^{-1} to 0.5 Å^{-1}. The obtained two-dimensional SANS patterns were reduced to be on the absolute scale using a protocol developed at NIST.[48]

Neutron spin echo (NSE)

NSE experiments were performed using the NGA-NSE spectrometer at NIST.[49,50] The selected q range was from 0.03 Å^{-1} to 0.16 Å^{-1} with the use of 6 Å, 8 Å and 11 Å neutron wavelengths. Fourier times, t, spanned from 0.2 ns to 100 ns. The tail-contrasted-matched samples were subjected to measurements in a 4 mm thick cell at 50 °C and the protiated samples in a 1 mm-thick cell at 54 °C. The obtained NSE signal was corrected for instrument resolution and solvent background to obtain the intermediate scattering function, $I(q,t)/I(q,0)$, using the software, DAVE[51].

4 Results and Discussion

Phase behavior

As already discussed in literature,[9,10,12,13] incorporating n-alkanes into lipid bilayers changes the lipid melting transition temperature T_m. The shifts in melting temperature are caused by the enthalpic stabilization due to enhanced packing of alkyl chains in the gel phase.[10] In the present study, some of the thermal anomalies were broadened by the n-alkane incorporation as shown in Fig. 2a and it was difficult to determine the onset temperatures. Here we treat the peak temperatures as T_m. T_m of pure DPPC and DPPC/n-alkane (DPPC : n-alkane = 6 : 4 (mol : mol)) bilayers is shown in Fig. 2b. For C8 and C10, the values of T_m are lower than that of pure DPPC, while T_m becomes increases with added C14. For the present work, it is important to understand the effects of n-alkanes on the phase transition temperature because the elastic properties are known to show anomalies at $T - T_m < 10$ °C.[52,53] All the other measurements in this study were performed at temperatures in the range $T - T_m \geq 10$ °C as stated in the section of sample prepartion. In the range of $T - T_m \geq 10$ °C, the elastic properties still have gradual dependence on temperature.[54] It is necessary to consider the differences in reduced temperature when discussing the measured elastic moduli. However, the results for pure DPPC and C12 can be directly compared without competing temperature effects since their T_m are almost the same.

Bilayer structure

The SAXS profiles of LUVs are shown in Fig. 3a. In the measured q range, the scattered intensity is dominated by the bilayer form factor. The characteristic first hump at the lowest-q corresponds to the main peak originated from the bilayer form factor followed by oscillatroy scattering as q gets higher. The dip location in the scattering profile relates to the bilayer thickness. The dip in the range of 0.2 Å$^{-1} < q < 0.3$ Å^{-1} shifts to lower q as the chain length of n-alkane increases, which indicates an increase in the bilayer thickness.

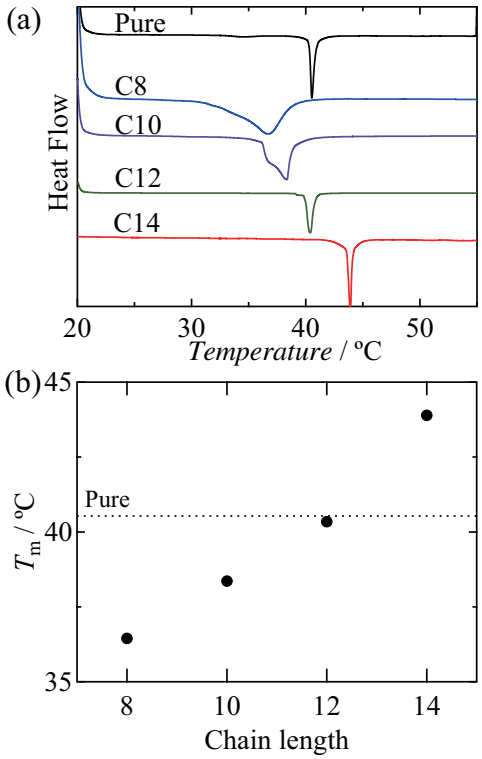

Fig. 2 (a) DSC traces of pure DPPC and DPPC/n-alkane (DPPC : n-alkane = 6 : 4 (mol : mol)) bilayers on the heating processes of the third cycle at a rate of 2 °C min^{-1}. (b) T_m determined from the peak temperatures of DSC traces in (a). Dotted line is T_m of the pure DPPC bilayer.

To quantify the changes in bilayer thickness with n-alkane length, we used a model of a core and five-shells,[55] as schematically shown in Fig. 1a, to fit the SAXS profiles. In the model, the lipid bilayer is represented by five shells that are each characterized by a thickness and electron density, and the total thickness of the three central shells is taken as d_c, the bilayer hydrocarbon thickness. Polydispersity was included into the core radius (radius of a vesicle) and the thickness of the central shell. The obtained d_c increased with increasing the n-alkane length, as shown in Fig. 3b.

The increase of the bilayer thickness, though, seems not significant. The incorporated n-alkanes can align parallel to the lipid alkyl chains or locate in the center of the bilayer. Parallel alignment is seen upon addition of several classes of small molecules including cholesterol, n-alkanes and n-alkane derivatives.[5,10,12,56] Assuming all of the incorporated n-alkanes are condensed at the central part of the bilayer and that neither the area per lipid nor specific volume of components are change upon mixing, the expected change in bilayer thickness is shown as the dot-

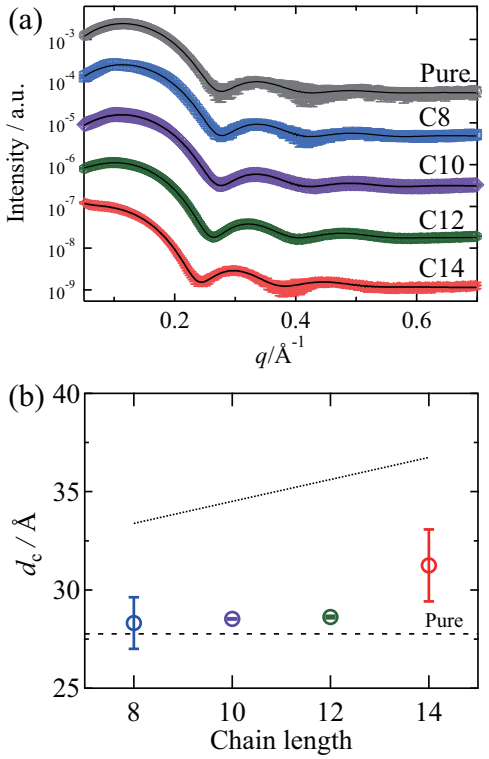

Fig. 3 (a) SAXS profiles of pure DPPC and DPPC/*n*-alkane mixtures (DPPC : *n*-alkane = 6 : 4 (mol : mol)) bilayers obtained at 54 °C. Error bars represent ±1 standard deviation, and the confidence intervals are 1.96 times of the error bars throughout the paper. Fitting results are the solid lines. (b) Plot of d_c obtained from fitting to the SAXS profiles. Broken line : d_c of the pure DPPC bilayer. Dotted lines : Calculated d_c assuming that all the incorporated *n*-alkane locates in the central plane of the bilayers.

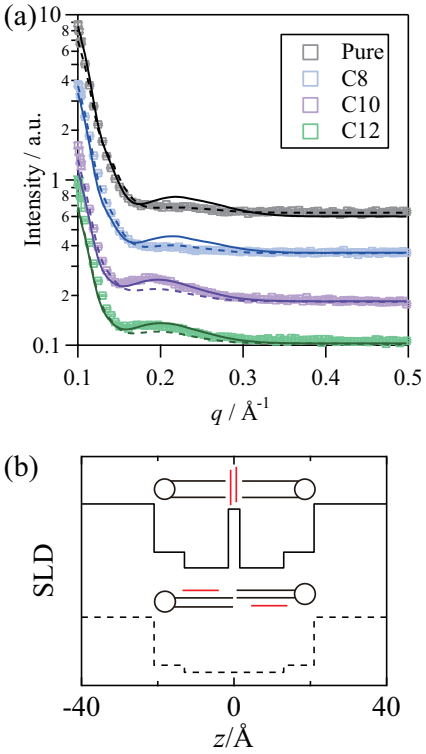

Fig. 4 (a) SANS profiles of DPPC and (protiated DPPC) : (deuterated *n*-alkane) = 6 : 4 (mol) bilayers obtained at 54 °C. Error bars represent ±1 standard deviation and are smaller than the plots. Solid and broken lines show the models at the top and bottom in (b), respectively. (b)Schematics of the contrast of bilayers consist of protiated DPPC and deuterated *n*-alkanes (red) in D_2O prepared for SANS. top : the contrast when deuterated *n*-alkanes locate in the midsurface. bottom : the contrast in the case for parallel alignment of deuterated *n*-alkanes.

ted line in Fig. 3b. All of the experimentally measured d_c are smaller than these calculated values. The smaller experimental d_c compared to the calculated values suggests that most *n*-alkanes align parallel to the acyl chains of the lipids. It is also possible that the area per molecule changes with *n*-alkane incorporation. Although the literature suggests that the total area per lipid increases upon addition of organic molecules such as cholesterol and drugs[57–61], it does not change significantly when the *n*-alkanes are absorbed into the center of the bilayer.[19,20] Compared to the other *n*-alkanes studied, addition of C14 leads to the greatest increase in d_c and the measured value is closest to the calculated value. The significant increase in thickness suggests that around 30 % of the for C14 is located within the center plane of the membrane. The changes in bilayer structures with the other *n*-alkanes are much smaller, and additional experiments were needed to determine where they are located within the bilayer.

To clarify the *n*-alkane location in the cases for C8, C10 and C12, we performed SANS experiments with the pure protiated DPPC bilayer and deuterated *n*-alkanes in D_2O. The calculatd SLD profiles are illustrated in Fig. 4b. Depending on the location of *n*-alkane, the scattering pattern should change significantly and we may qualitatively discuss the location of the molecules. Fig. 4a shows SANS profiles for pure, C8, C10, and C12 incorporated bilayers. In the cases of the pure DPPC bilayer and the DPPC/C8 bilayer, the SANS profiles are flat around 0.2 $Å^{-1}$, but there is a hump in the cases of DPPC with C12 and C10. As schematically depicted in Fig. 4b, localization of the *n*-alkanes at the central part of the bilayer can significantly change the SLD profile. Therefore, the hump for C10 and C12 arises from the localization of the incorporated *n*-alkanes at the center of bilayers. Fig. 4a also shows the fit results with solid and broken lines for the different SLD conditions. The dashed line shows the profile for the parallel configurations for the incorporated *n*-alkanes, while the solid lines represent the case a portion of incorporated *n*-alkane is located in the central plane of the bilayer. In these fitting, we fixed the parameters other than the scattering length densities of the leaflets. In the pure DPPC and DPPC/C8 bilayer, the broken lines fit the SANS profile better than the solid lines, indicating the structureless SLD profile in the hydrophobic region. It is reasonable for the pure DPPC bilayer since the hydrophobic region consists of only protiated chains. The fitting result indicates that the deuterated C8 are located parallel to the lipid alkyl tails in the bilayer which is consistent with the small increase in thickness measured with SAXS. On the other hand, the SANS data for added C10 and C12 were approximated better by the solid lines, suggesting that a portion of the *n*-alkanes distribute in the central plane of bilayers. C14 is expected to locate in the central plane

considering the significant increase in d_c in DPPC/C14 bilayers and the chain length dependence that other physicochemical parameters exhibit.[9,10,13,62]

This trend with *n*-alkane length is opposite to the previous observation by McIntosh,[13] where shorter chain *n*-alkanes caused a greater increase in the bilayer thickness. One potential difference between the results by McIntosh and the present systems is amount of incorporated *n*-alkane. Since McIntosh *et al.* saturated the lipid bilayer with *n*-alkane, the incorporated amount can differ depending on the *n*-alkane length. The incorporated amounts of *n*-alkanes are likely different depending on the chain length. Work by Gruen and Haydon[63] suggested that the location of the *n*-alkane within the bilayer also depended on the volume fraction, where low concentrations were distributed throughout the bilayer and, as the volume fraction increases, the distribution within the center of the bilayer plane also increases. This agrees with our experiment where we kept the mole fraction of *n*-alkane constant which leads to the volume fraction of 0.19, 0.22, 0.25 and 0.28 for C8, C10, C12 and C14, respectively. Thus, one possibility is that McIntosh *et al.* incorporated a larger volume fraction of shorter *n*-alkanes than longer *n*-alkanes. We also note that the *n*-alkane concentrations used in the present studies are significantly higher than clinically relevant anesthesia concentrations, which are estimated at an approximate mole ratio of 0.02 to 0.05.[64,65] The high *n*-alkane concentrations were used to compare with previous experimental results, but the effects may not extrapolate to the low concentrations used in other applications.

The present results are for liquid-crystalline phase bilayers. Our previous results focused on gel phase DPPC, where the *n*-alkane aligned parallel to the lipid alkyl chains due to the enthalpic gain.[10] The parallel alignment in the gel phase was seen in the decrease in the lattice constant of lipid alkyl chain with increasing incorporation ratio of *n*-alkanes and also showed a chain length dependence.[9,10,12] Our present results suggest that the location of the *n*-alkane within a membrane differs depending on the lipid phase state and whether the lipid is in the gel or liquid-crystalline phases.

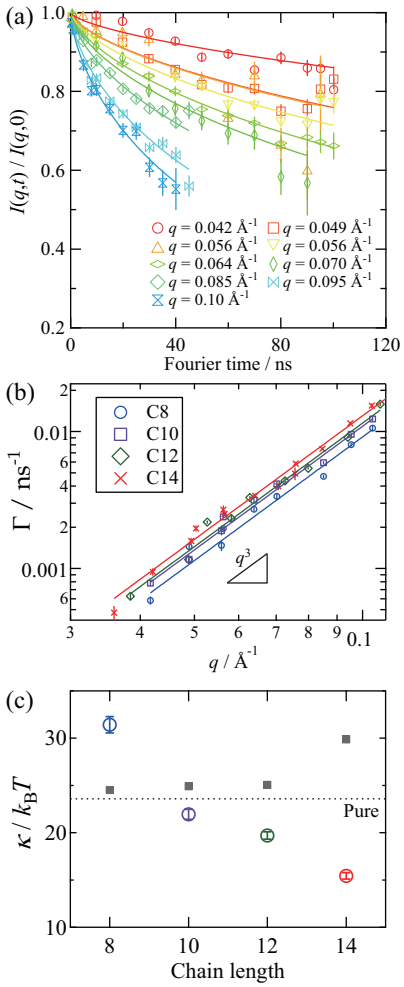

Fig. 5 (a) Intermediate scattering function $I(q,t)/I(q,0)$ of the fully protiated DPPC: C8 (6 : 4 mol) bilayers measured by NSE at 54 °C. The solid lines are the fits by Eq. 1. (b) The q dependence of Γ for the fully protiated samples (DPPC : *n*-alkane = 6 : 4 (mol : mol)) measured at 54 °C. The solid lines are the fit results to Eq. 2. (c) Circles : experimentally determined κ from fits to the NSE data at 54 °C. Squares : Calculated κ from Eq. 3 based on the measured change in bilayer thickness and assuming K_A and β are constant and equal to the values for pure DPPC.

Bending elasticity

Fig. 5a shows the measured $I(q,t)/I(q,0)$ for the fully protiated DPPC/C8 bilayers. The C8 data in the figure and all other samples studied here are well fit by the ZG theory (Eq. 1). These fits suggest that the dynamics captured for the *n*-alkane incorporated bilayers follow the same single membrane undulation model used to describe pure lipid bilayers. This result is more evident from the q-dependence of Γ estimated from the $I(q,t)$. Fig. 5b shows the decay constant Γ extracted from the $I(q,t)/I(q,0)$, which show a q^3 dependence for all of the lipid : *n*-alkane mixtures. We used Eq. 2 to estimate the value of κ, and the fit results are depicted in Fig. 5b as solid lines.

The extracted bending modulus κ values are plotted in Fig. 5c. The bending modulus for C8 incorporated bilayers is larger than that of the pure DPPC, while κ decreases with increasing *n*-alkane length such that C12 and C14 bilayers are softer than pure DPPC. The softening of the bilayer with added *n*-alkane is unexpected based on the measured increase in bilayer thickness. As we showed in the structure section, the bilayer thickness is larger when *n*-alkane is incorporated and increases with increasing *n*-alkanes chain length. Eq. 3 predicts a quadratic increase of κ with increasing d_c. When we calculate the values of κ using the experimentally measured d_c values and assume constant values for K_A and β in Eq. 3, we would expect κ to follow the gray squares in Fig. 5c. In other words, if the changes in κ were due solely to the changes in bilayer structure, then κ for the C12 and C14 bilayers would increase compared to pure DPPC. Therefore, our results suggest that either K_A or β (or both) are changing and leading to a decrease in κ with *n*-alkane incorporation.

As suggested in the phase behavior section, another potential source of the change in κ is the differences in relative temperature. It is known that the values of κ in the gel phase are about an order of magnitude larger than the values in the fluid

phase,[35,37,66] and that κ decreases further with increasing T above T_m. However, our measurements of T_m indicate that T_m increases as the chain length of *n*-alkane increases. Therefore, the longer *n*-alkanes are closer to T_m and should have a larger value of κ. As this is not the case for our experimental results, the change of T_m with the chain length of *n*-alkane cannot explain the changes in κ.

Interleaflet Coupling

As we stated in the Theory section, K_A determines the thickness fluctuation amplitude. Thus by measuring the thickness fluctuations with NSE, we are able to estimate the effects of adding *n*-alkanes on K_A. Fig. 6a shows the $I(q,t)/I(q,0)$ measured for tail-deuterated-DPPC/deuterated-C10 bilayer with which the scattering length density of the hydrophobic region matched to D_2O. The decay was well fit accordingly to Eq. 1. Fitting of the $I(q,t)/I(q,0)$ for the other tail-deuterated-DPPC/deuterated-*n*-alkane systems were successfully done in the same way and the values of Γ are shown in Fig. 6b. If the dynamics are solely coming from the membrane height (bending) undulations, Γ/q^3 should be a constant with q. A deviation from the q^3 scaling is seen for pure DPPC and DPPC/*n*-alkane systems except for C8. The excess peak is centered around $q_0 = 0.07$ Å^{-1}, which moves to lower q as the *n*-alkane length increases. The peak shift reflects the increase in the bilayer thickness with *n*-alkane elongation observed with SAXS and SANS. In the case of C8, however, possible reasons for missing the "excess" signal are the broadening of the peak (increase in ξ^{-1}) and/or the weakening of the peak intensity (increase in τ_{TF}). The average value of Γ/q^3 for the tail-contrast-matched DPPC/C8 bilayers is 13 Å^3/ns^{-1}, while it is 9 Å^3/ns^{-1} for the fully protiated bilayers. This difference indicates that the width (ξ^{-1}) of the peak was broadened upon incorporation of C8. However, we could not quantify how broad the peak would be from the present data.

Eq. 4 was employed to fit Γ/q^3 in Fig. 6b for the present data except for C8 where q_0 and κ are fixed based on the measured SANS of the tail-contrast-matched samples (data not shown) and NSE from the fully protiated samples (See Fig. 5c), respectively. Also, we applied the instrumental q resolution estimated using the pure DPPC data to the other data sets by following the method applied before.[24] Thus, the only fit parameters are τ and ξ.

The fit results for ξq_0 are shown in Fig. 6c, which is proportional to the inverse of the thickness fluctuation amplitude. As the value of ξq_0 is smaller for the DPPC/*n*-alkane mixtures than pure DPPC, the *n*-alkane incorporated bilayers have a larger thickness fluctuation amplitude. This trend indicates that the *n*-alkane incorporated bilayers are in general more compressible than the pure DPPC bilayers.

The ξq_0 increases with increasing *n*-alkane length from C10 to C14, suggesting K_A increases per Eq. 7. Fluctuation data shows that the trend in K_A is opposite to the trend in κ, i.e. the membrane is less compressible, yet more flexible with increasing d_c. These trends in moduli are only possible if β also increases (Eq. 3) and the leaflets are less coupled with added *n*-alkane. Namely, the data suggest that DPPC/*n*-alkane membranes are behaving more like two uncoupled leaflets than the pure DPPC bilayer. Our attempt to quantitatively extract β from the observed experimental parameters, though, was not reliable. While we were able to estimate that changes in A_0 were small from our structural data, we were not able to extract a definitive value which is needed to calculate β (Eq. 7). Also it is possible that some other internal membrane dissipation mechanisms might also contribute to the measured NSE data and therefore reduce the reliability of our estimates of the elastic parameters. Nevertheless, while we only qualitatively discuss the changes in β in the present work, we hope our results motivate future experiments and simulations to provide a more thorough understanding of coupling in lipid bilayers.

The structural data provide additional insights into the *n*-alkane effects on the membrane dynamics. The structural data showed that a part of C12 and C14 *n*-alkanes were also located in the center of the bilayer, physically separating the two DPPC leaflets, which may suggest that decreasing interactions between leaflets will also affect the dynamics. The data presented here for *n*-alkanes show similar behavior to the work by Shchelokovskyy *et al.* where addition of HIV-fusion peptide also increased β.[23] Together these results suggest that decreasing the interactions between the bilayer leaflets will impact the membrane dynamics and point to an additional mechanism through which additives can influence the membrane properties.

5 Conclusion

In this study, we used neutron scattering techniques to probe the effects of *n*-alkanes on the structure and dynamics of lipid bilayers. Combining measurements of the bending and thickness fluctuations suggested that the coupling between the leaflets in a bilayer is weakened with added *n*-alkanes. Due to this decoupling, the bilayer becomes easier to bend despite being thicker. The decrease in coupling seems to correspond to the *n*-alkane location within the membrane, suggesting that decreasing the physical interactions between the leaflets decreases the coupling.

Our results are also striking as an investigation into the effects of additives on lipid bilayers. Previous work has focused on the effects of *n*-alkanes on the lipid phase behavior and bilayer structure. Our results emphasize that adding *n*-alkanes can have significant effects on the membrane dynamics as well. Moreover, our results for *n*-alkanes suggest that these effects will depend on where the additive is located within the membrane. Other small organic molecules will likely have significant effects on biomembrane dynamics. Our results allude to the possibility that the presence of small molecules in biological membranes also controls the membrane dynamics, such as bending, thickness fluctuations and slipping between leaflets, to maintain the functionality of the membrane.

Conflicts of interest

There are no conflicts to declare.

Acknowledgement

Access to the Neutron Spin Echo Spectrometer was provided by the Center for High Resolution Neutron Scattering, a partnership

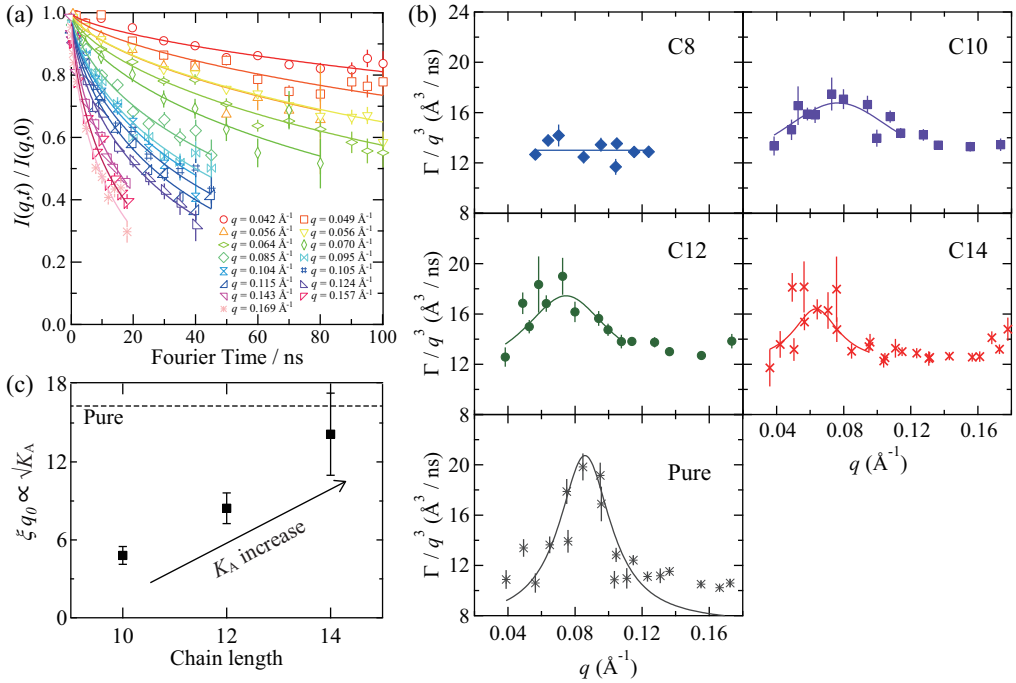

Fig. 6 (a) Intermediate scattering function $I(q,t)/I(q,0)$ of the tail-contrast-matched DPPC/C10 (6/4 mol) bilayers measured by NSE at 50 °C. The solid lines are the fits to Eq.1. (b) The q dependence of Γ/q^3 for the headgroup-highlighted samples (DPPC : n-alkane $= 6:4$ (mol : mol)) measured at 50 °C. The solid lines are fitting results of Eq. 4. Pure: the case of the pure DPPC bilayers[24] (c) ξq_0 of the n-alkane incorporated DPPC bilayers at 50 °C.

between the National Institute of Standards and Technology and the National Science Foundation under Agreement No. DMR-1508249. H.U. was supported by JSPS KAKENHI Grant Number 18J12652. M.H. was supported by JSPS KAKENHI Grant Number 18K03555 and 19H05717. M.N. acknowledges funding support of cooperative agreement 70NANB15H259 from NIST, U.S. Department of Commerce. Travel expenses for the SANS and NSE experiment performed at NIST, USA, were supported by General User Program for Neutron Scattering Experiments, Institute for Solid State Physics, The University of Tokyo (proposal no. 18560 and 17902), at JRR-3, Japan Atomic Energy Agency, Tokai, Japan. Certain trade names and company products are identified in order to specify adequately the experimental procedure. In no case does such identification imply recommendation or endorsement by the National Institute of Standards and Technology, nor does it imply that the products are necessarily the best for the purpose.

Notes and references

1 R. Phillips, T. Ursell, P. Wiggins and P. Sens, *Nature*, 2009, **459**, 379–385.
2 B. Ladbrooke, R. Williams and D. Chapman, *Biochim. Biophys. Acta*, 1968, **150**, 333 – 340.
3 R. Demel and B. D. Kruyff, *Biochim. Biophys. Acta*, 1976, **457**, 109 – 132.
4 T. P. McMullen and R. N. McElhaney, *Biochim. Biophys. Acta*, 1995, **1234**, 90 – 98.
5 H. Ohvo-Rekilä, B. Ramstedt, P. Leppimäki and J. P. Slotte, *Prog. Lipid Res.*, 2002, **41**, 66 – 97.
6 O. Edholm and J. Nagle, *Biophys. J.*, 2005, **89**, 1827–32.
7 T. Mills, J. Huang, G. Feigenson and J. Nagle, *Gen. Physiol. Biophys.*, 2009, **28**, 126–39.
8 N. Tamai, T. Izumikawa, S. Fukui, M. Uemura, M. Goto, H. Matsuki and S. Kaneshina, *Biochim. Biophys. Acta*, 2013, **1828**, 2513 – 2523.
9 M. Hishida, R. Yanagisawa, H. Usuda, Y. Yamamura and K. Saito, *J. Chem. Phys.*, 2016, **144**, 041103.
10 M. Hishida, A. Endo, K. Nakazawa, Y. Yamamura and K. Saito, *Chem. Phys. Lipids*, 2015, **188**, 61 – 67.
11 H. Usuda, M. Hishida, Y. Yamamura and K. Saito, *Langmuir*, 2016, **32**, 5966–5972.
12 H. Usuda, M. Hishida, Y. Yamamura and K. Saito, *Chem. Lett.*, 2018, **47**, 1512–1514.
13 T. McIntosh, S. Simon and R. MacDonald, *Biochim. Biophys. Acta*, 1980, **597**, 445 – 463.
14 D. Haydon, B. Hendry, S. Levinson and J. Requena, *Biochim. Biophys. Acta*, 1977, **470**, 17 – 34.
15 S. White, *Biophys. J.*, 1978, **23**, 337 – 347.
16 J. Pope, L. Walker and D. Dubro, *Chem. Phys. Lipids*, 1984, **35**, 259 – 277.
17 D. A. Haydon, B. M. Hendry, S. R. Levinson and J. Requena, *Nature*, 1977, **268**, 356–358.
18 G. D. Bothun, B. L. Knutson, H. J. Strobel and S. E. Nokes, *Coll. Surf. A*, 2006, **279**, 50 – 57.
19 D. Gruen and D. Haydon, *Biophys. J.*, 1980, **30**, 129 – 136.
20 S. H. White, G. I. King and J. E. Cain, *Nature*, 1981, **290**, 161–163.
21 D. Boal, *Mechanics of the Cell*, Cambridge University Press,

2nd edition, 2002.
22 W. Rawicz, K. Olbrich, T. Mcintosh, D. Needham and E. Evans, *Biophys. J.*, 2000, **79**, 328–339.
23 P. Shchelokovskyy, S. Tristram-Nagle and R. Dimova, *New J. Phys.*, 2011, **13**, 25004.
24 M. Nagao, E. G. Kelley, R. Ashkar, R. Bradbury and P. D. Butler, *J. Phys. Chem. Lett.*, 2017, **8**, 4679–4684.
25 A. G. Zilman and R. Granek, *Phys. Rev. Lett.*, 1996, **77**, 4788–4791.
26 W. Helfrich, *Z. Naturforsch. C*, 1973, **28**, 693–703.
27 J.-H. Lee, S.-M. Choi, C. Doe, A. Faraone, P. A. Pincus and S. R. Kline, *Phys. Rev. Lett.*, 2010, **105**, 038101.
28 Z. Yi, M. Nagao and D. Bossev, *J. Phys., Condens. Matter*, 2009, **21**, 155104.
29 T. Takeda, Y. Kawabata, H. Seto, S. Komura, S. Ghosh, M. Nagao and D. Okuhara, *J. Phys. Chem. Solids*, 1999, **60**, 1375 – 1377.
30 M. C. Watson and F. L. Brown, *Biophys. J.*, 2010, **98**, L9 – L11.
31 U. Seifert and S. A. Langer, *Europhys. Lett.*, 1993, **23**, 71–76.
32 E. G. Kelley, P. D. Butler and M. Nagao, in *Collective Dynamics in Model Biological Membranes Measured By Neutron Spin Echo Spectroscopy*, De Gruyter, Berlin, Boston, 2019, ch. 4, pp. 131–176.
33 R. J. Bingham, S. W. Smye and P. Olmsted, *Europhys. Lett.*, 2015, **111**, 18004.
34 R. Bradbury and M. Nagao, *Soft Matter*, 2016, **12**, 9383–9390.
35 E. G. Kelley, P. D. Butler and M. Nagao, *Soft Matter*, 2019, **15**, 2762–2767.
36 M. Nagao, *Phys. Rev. E*, 2009, **80**, 031606.
37 A. C. Woodka, P. D. Butler, L. Porcar, B. Farago and M. Nagao, *Phys. Rev. Lett.*, 2012, **109**, 058102.
38 M. Nagao, S. Chawang and T. Hawa, *Soft Matter*, 2011, **7**, 6598–6605.
39 V. Lee and T. Hawa, *J. Chem. Phys.*, 2013, **139**, 124905.
40 R. Ashkar, M. Nagao, P. D. Butler, A. C. Woodka, M. K. Sen and T. Koga, *Biophys. J.*, 2015, **109**, 106 – 112.
41 J.-M. Y. Carrillo, J. Katsaras, B. G. Sumpter and R. Ashkar, *J. Chem. Theory Comput.*, 2017, **13**, 916–925.
42 E. Lindahl and O. Edholm, *Biophys. J.*, 2000, **79**, 426 – 433.
43 C.-H. Lee, W.-C. Lin and J. Wang, *Phys. Rev. E*, 2001, **64**, 020901.
44 G. Bryant, M. B. Taylor, T. A. Darwish, A. M. Krause-Heuer, B. Kent and C. J. Garvey, *Coll. Surf. B*, 2019, **177**, 196 – 203.
45 J. Ilavsky, *J. Appl. Crystallogra.*, 2012, **45**, 324–328.
46 C. J. Glinka, J. G. Barker, B. Hammouda, S. Krueger, J. J. Moyer and W. J. Orts, *J. Appl. Crystallogra.*, 1998, **31**, 430–445.
47 S.-M. Choi, J. Barker, C. Glinka, Y. Cheng and P. Gammel, *J. Appl. Crystallogra.*, 2000, **33**, 793–796.
48 S. R. Kline, *J. Appl. Crystallogra.*, 2006, **39**, 895–900.
49 N. Rosov, S. Rathgeber and M. Monkenbusch, in *Neutron Spin Echo Spectroscopy at the NIST Center for Neutron Research*, American Chemical Society, 1999, ch. 7, pp. 103–116.
50 M. Monkenbusch, R. Schätzler and D. Richter, *Nucl. Instrum. Meth. Phys. Res. A*, 1997, **399**, 301 – 323.
51 R. Dimeo, R. Tumanjong Azuah, L. R. Kneller, Y. Qiu, P. L. W. Tregenna-Piggott, C. Brown and J. R. D. Copley, *J. Res. NIST*, 2009, **114**, 341.
52 N. Chu, N. Kučerka, Y. Liu, S. Tristram-Nagle and J. F. Nagle, *Phys. Rev. E*, 2005, **71**, 041904.
53 R. Dimova, *Adv. Colloid Interface Sci.*, 2014, **208**, 225 – 234.
54 J. Pan, S. Tristram-Nagle, N. Kučerka and J. F. Nagle, *Biophys. J.*, 2008, **94**, 117 – 124.
55 M. Hirai, H. Iwase, T. Hayakawa, M. Koizumi and H. Takahashi, *Biophys. J.*, 2003, **85**, 1600–1610.
56 E. Drolle, N. Kučerka, M. Hoopes, Y. Choi, J. Katsaras, M. Karttunen and Z. Leonenko, *Biochim. Biophys. Acta*, 2013, **1828**, 2247 – 2254.
57 O. Edholm and J. F. Nagle, *Biophys. J.*, 2005, **89**, 1827 – 1832.
58 Y. Nademi, S. Amjad Iranagh, A. Yousefpour, S. Z. Mousavi and H. Modarress, *J. Chem. Sci.*, 2014, **126**, 637–647.
59 S. Chiu, E. Jakobsson, R. J. Mashl and H. L. Scott, *Biophys. J.*, 2002, **83**, 1842 – 1853.
60 C. Hofsäß, E. Lindahl and O. Edholm, *Biophys. J.*, 2003, **84**, 2192 – 2206.
61 E. Falck, M. Patra, M. Karttunen, M. T. Hyvönen and I. Vattulainen, *Biophys. J.*, 2004, **87**, 1076 – 1091.
62 H. Kamaya, N. Matubayasi and I. Ueda, *J. Phys. Chem.*, 1984, **88**, 797–800.
63 D. Gruen and D. Haydon, *Biophys. J.*, 1981, **33**, 167 – 187.
64 R. S. Cantor, *Biophys. J.*, 2001, **80**, 2284 – 2297.
65 N. P. Franks and W. R. Lieb, *Proc. Natl. Acad. Sci.*, 1986, **83**, 5116–5120.
66 H. Seto, N. L. Yamada, M. Nagao, M. Hishida and T. Takeda, *Euro. Phys. J. E*, 2008, **26**, 217.